J. Fluid Mech. (1999), *vol.* 393, *pp.* 309–332. Printed in the United Kingdom

© 1999 Cambridge University Press

Three-dimensional large-amplitude drop oscillations: experiments and theoretical analysis

By HISAO AZUMA† AND SHOICHI YOSHIHARA

National Aerospace Laboratory, 7-44-1 Jindaiji-higashimachi, Chofu, Tokyo

(Received 24 October 1997 and in revised form 13 April 1999)

Three-dimensional large-amplitude oscillations of a mercury drop were obtained by electrical excitation in low gravity using a drop tower. Multi-lobed (from three to six lobes) and polyhedral (including tetrahedral, hexahedral, octahedral and dodecahedral) oscillations were obtained as well as axisymmetric oscillation patterns. The relationship between the oscillation patterns and their frequencies was obtained, and it was found that polyhedral oscillations are due to the nonlinear interaction of waves.

A mathematical model of three-dimensional forced oscillations of a liquid drop is proposed and compared with experimental results. The equations of drop motion are derived by applying the variation principle to the Lagrangian of the drop motion, assuming moderate deformation. The model takes the form of a nonlinear Mathieu equation, which expresses the relationships between deformation amplitude and the driving force's magnitude and frequency.

1. Introduction

Liquid drop oscillation has attracted the attention of many scientists since the 19th century, since it is not only an interesting basic phenomenon but is also important in such diverse areas as nuclear physics, cloud physics and chemical engineering. Since it has become possible to conduct experiments in microgravity, understanding liquid drop oscillation has become more important, not only from an academic viewpoint but also for the practical aspects of material processing in containerless levitation and measurement of the physical properties of molten materials in space. In a microgravity environment, a free liquid assumes a spherical shape due to surface tension and it is easy to levitate and manipulate a relatively large liquid drop without a container. This is one of the advantages of the space environment. Understanding the nature of drop oscillations is indispensable for future applications of containerless processing. In addition, nonlinear effects resulting from the interaction of finite-amplitude waves are of interest from physical and mathematical points of view, and experimental realization of large-amplitude oscillations is useful for the study of these effects.

The first large-amplitude drop oscillation experiments were conducted by acoustically exciting a drop suspended in an immiscible liquid (a mixture of silicone oil and carbon tetrachloride suspended in distilled water) in 1 g conditions (Trinh & Wang 1982). These experiments showed oscillating patterns in the $l = 2$, 3, 4 axisymmetric ($m = 0$) modes and also showed the dependence of the amplitude of oscillation of the second mode on oscillation frequency.

† Present address: Osaka Prefecture University, 1-1 Gakuen-Cho, Sakai, Osaka, Japan.

https://doi.org/10.1017/S0022112099005728 Published online by Cambridge University Press

Finite-amplitude, axially symmetric free oscillations of small (0.2 mm) droplets have been obtained by breaking up a laminar jet, and the amplitude variations of the oscillations have been measured (Becker, Hiller & Kowalewski 1991). In these experiments, in which oscillations undergo natural decay, it was found that when the amplitude of natural oscillations of the fundamental mode exceeds approximately 10% of the droplet radius, typical nonlinear effects occurred such as the dependence of the amplitude on oscillation frequency, asymmetry of the oscillation amplitude, and interactions between modes.

Polyhedral-shaped oscillations of a drop suspended in an aqueous solution were obtained by applying periodic mechanical excitation (Arai, Adachi & Takaki 1991). A drop of orthotoluidine with a radius of approximately 2 cm was suspended in a dilute aqueous sugar solution in a square container. A thin rod connected to a loudspeaker was placed in contact with the drop from above, producing an oscillation. Two rods were used to obtain asymmetric oscillations.

Egry, Lohoefer & Sauerland (1993) measured oscillations of an electromagnetically levitated metal drop in both 1 g and microgravity conditions in order to measure surface tension and viscosity. Surface tension was determined by measuring the frequency of small-amplitude oscillations excited by an electromagnetic pulse.

With regard to theoretical works, a linear theory of small-amplitude oscillations of an inviscid drop was first proposed by Rayleigh (1879), who expressed the fundamental modes in terms of Legendre polynomials. Lamb (1932, Art 355) looked at the effect of low viscosity, and an equation describing the effect of arbitrary viscosity on the infinitesimal-amplitude oscillation of drops was derived by Reid (1960). Moderate-amplitude axisymmetric oscillations of incompressible inviscid drops were analysed by Tsamopoulos & Brown (1983) using a Poincaré–Lindstedt expansion technique, and the effects of mode coupling at the second order in amplitude on drop shape and velocity potential were predicted. Natarajan & Brown (1986, 1987) considered quadratic and third-order resonance in three-dimensional drop oscillations using equations describing the interaction of the modes, which were derived by applying the variational principle to the appropriate Lagrangian.

Lundgren & Mansour (1988) made numerical studies of nonlinear oscillation and other motions of large axially symmetric weakly viscous liquid drops in zero gravity using a boundary-integral method. They showed that a weak viscosity has a relatively large effect on resonant-mode coupling phenomena. Becker *et al.* (1991) proposed a nonlinear model for inviscid droplet oscillations which predicted the nonlinear effects they found in their experiments. Feng & Beard (1991) analysed the three-dimensional oscillation characteristics of a charged drop in an insulating medium and in an electrostatic field. They observed a fine structure in the characteristic frequency spectrum of the oscillations of electrostatically deformed drops by means of the multiple-parameter perturbation method. They also discovered the dependence of oscillation frequency on electric field strength and on the degree and the rank of spherical harmonics, indicating that the removal of degeneracy may be considered a consequence of symmetry breaking. Basaran (1992) and Becker, Hiller & Kowalewskii (1994) considered nonlinear viscous liquid drop oscillations and showed that finite viscosity has a large effect on mode coupling.

It can be seen that large-amplitude oscillations over a wide frequency range, especially three-dimensional oscillations, have not been realized experimentally prior to this present work; only some numerical simulations (Lundgren & Mansour 1988) have been conducted. A different experimental method from those mentioned above was used in this study, and the electrically driven liquid drop excitation method under

https://doi.org/10.1017/S0022112099005728 Published online by Cambridge University Press

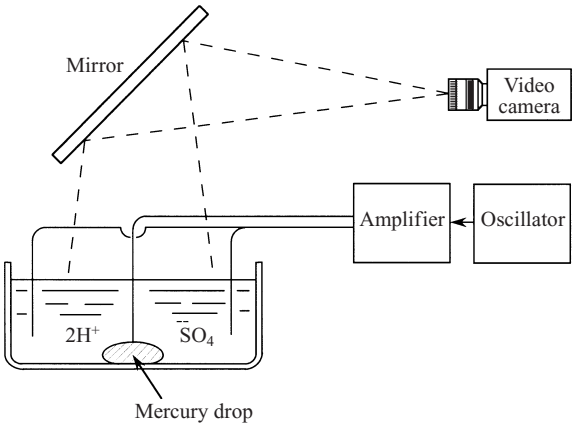


FIGURE 1. Schematic of the experimental set-up.

low-gravity conditions is a feature of these experiments. This method allows the imposition of an oscillation of arbitrary frequency on an arbitrarily sized drop and also makes it easy to conduct three-dimensional oscillation experiments in a short-duration low-gravity environment, obtained by dropping the experimental apparatus.

2. Experiment

2.1. *Experimental apparatus*

A schematic of the experimental apparatus used in 1 g conditions is shown in figure 1. The drop had to be conducting, and so mercury was chosen as the liquid. The mercury drop was immersed in an electrolytic solution (in this case 0.1 N sulphuric acid) on a flat plate. Through two electrodes, one in contact with the drop and another immersed in the electrolytic solution, an alternating signal of arbitrary voltage amplitude and frequency was applied between the drop and the solution.

For two-dimensional oscillations, experiments were conducted by varying the frequency of a constant-amplitude (5, 10, 20, 30 V) applied alternating signal and the resulting oscillations of the drop were observed using a standard video camera or a high-speed (1000 frames/s) video recorder.

Experiments on three-dimensional oscillations were conducted using a 10 m high drop tower giving a drop time of 1.4 s. After an initial oscillation of the capsule containing the experimental apparatus caused by its separation from a beam, the acceleration level decreases to less than 10^{-3} g. At impact, after 1.4 s of free fall, the capsule receives an acceleration of more than 30 g. The drop oscillation experiments were conducted during a 1 s interval corresponding to a very low gravity level. The apparatus in the capsule and the cylindrical experiment container are shown in figures 2(*a*) and 2(*b*). Under 1 g conditions, a mercury drop is placed at the centre of the bottom of the cylindrical container filled with dilute sulphuric acid. Just after the release of the capsule, the mercury drop becomes spherical and floats upwards due to its repulsive force. An alternating voltage signal (20, 30 V) is applied through a wire running along the axis of the container and four wires immersed in the sulphuric acid: 20 V were applied from 2 Hz to 14 Hz and 30 V from 14 Hz to 30 Hz to induce large-amplitude oscillations. The time required for the drop oscillation to reach a steady state was measured as about 1 s, leaving an interval of only 0.4 s during which steady drop oscillations could be observed in free fall. Drop behaviour was observed using two video cameras (30 frames/s with 1/250 s shutter speed, which is insufficient

https://doi.org/10.1017/S0022112099005728 Published online by Cambridge University Press

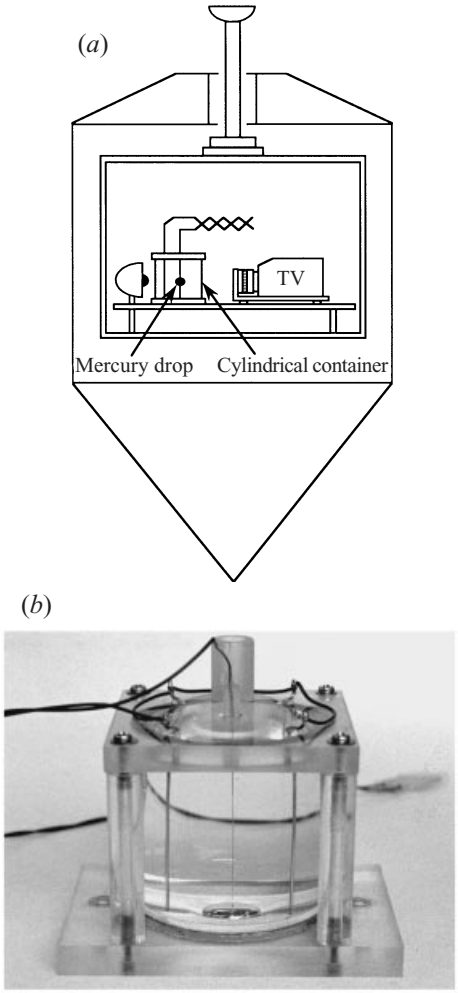


FIGURE 2. (*a*) Schematic of the drop capsule and the experimental set-up, and (*b*) a photo of the cylindrical container with the mercury drop on its bottom.

for observing high-frequency oscillations) set at right angles to each other. The highest measurable frequency of oscillation was limited to 30 Hz.

2.2. *Experimental method*

Due to potential difference, an electric charge is carried through the electrolytic solution onto the drop's surface and the amount of charge on the surface can easily be varied by changing the voltage of the applied alternating signal. The applied signal's voltage range was between 0 and 30 V over a frequency range of between 0 and 60 Hz. The drop may be oscillated at any frequency within this range.

The electric charge on the surface of the drop has the effect of reducing surface tension and so varying the electric charge causes a variation of the drop's surface tension, which is the superposition of surface tension in its usual meaning and an electrical force. A variation of surface tension is equivalent to a variation of applied pressure, and the variation of the electromechanical force drives drop oscillation, as shown in the analysis of § 3.3.2. The electromechanical force was measured as shown in figure 3(*a*) and an example of the measured electromechanical force variation

https://doi.org/10.1017/S0022112099005728 Published online by Cambridge University Press

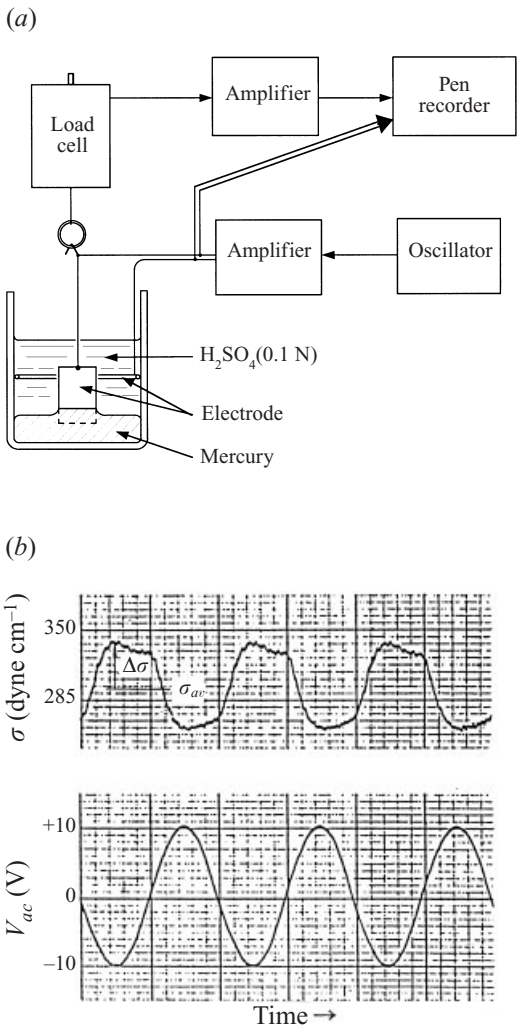


FIGURE 3. (*a*) Schematic of the method of measuring the mercury surface tension. (*b*) Measured surface tension and the applied voltage (5 Hz) as functions of time.

V_{ac} (V)	$\Delta\sigma$ (dyne cm^{-1})	$\Delta\sigma/\sigma_{av}$
$\pm$ 5	27	0.08
$\pm$10	36	0.11
$\pm$20	42	0.14

TABLE 1. Variation of the surface tension due to the 5 Hz applied voltage.

together with the applied alternating voltage is shown in figure 3(*b*). Although the measured force seems to contain higher harmonics caused by problems of the measuring technique, such as rapid surface deformation due to electromechanical force change (mercury tends to become spherical by increasing its surface tension), it seems reasonable to infer that the electromechanical force variation of the mercury is driven by the applied voltage and changes almost sinusoidally.

https://doi.org/10.1017/S0022112099005728 Published online by Cambridge University Press

Measurements of the variations of the electromechanical force $\Delta\sigma$ and the ratios of the measured values to the averaged electromechanical force $\Delta\sigma/\sigma_{av}$ are shown in table 1. Gas produced at the mercury surface and surface oscillations of the drop itself prevented precise measurement, especially with a 30 V applied alternating signal. The surface tension of mercury in sulphuric acid in the absence of an applied voltage was measured at 330 dyne cm^{-1}, which is much lower than the 482 dyne cm^{-1} surface tension of mercury in a nitrogen atmosphere (Tokyo Astronomical Observatory 1985). Applying an alternating voltage signal reduced the averaged apparent surface tension as shown in figure 3(*b*). Although estimation of the error of the measured surface tension is difficult, it is thought that the error of the ratio $\Delta\sigma/\sigma_{av}$ could be less than 10%.

Variation of the electromechanical force is thought to be caused by the variation of forces between the electric charges on the mercury surface. Although the precise mechanism is not clear, the result in figure 3(*b*) shows that it depends on a movement of electric charges onto the mercury surface. It is therefore considered that the force acting on the spherical liquid surface is almost point symmetrical even though the arrangement of the electrodes is not, as shown in figure 2(*b*). In addition to the electromechanical force, electrical stress is thought to act on the surface as a tension (Zhang & Basaran 1996) and this force is not point symmetric with respect to the centre of the mercury sphere. However, assuming the permittivity of the dilute sulphuric acid to be 100, the order of the electrical stress is estimated to be ~ 0.05, which is negligible compared to the measured surface tension variation (~ 40 dyne cm^{-1}), and so the effect of the electrical stress can be neglected.

2.3. *Experimental results for two-dimensional oscillations under normal gravity conditions*

Oscillation patterns were observed in a mercury drop of mass 13.6 g with a radius of 1.05 cm. The mercury drop is flattened by its own weight, and its oscillation is assumed to be quasi-two-dimensional.

In figure 4, the normalized maximum deformation of the drop from spherical shape ζ ($\zeta = R_{max}/R_0 - 1$) is shown with the corresponding applied voltage. The drop's amplitude variation is expressed as the ratio of the circumscribed circle radius of the deformed drop R_{max} to the normal circle radius R_0. Figure 3(*b*) shows that surface tension and applied voltage are in opposite phase while the surface tension is in phase with the drop's amplitude, but this was not always the case observed in the experiments.

Observations of oscillation patterns were made at 0.2 Hz increments of the applied signal frequency from 1 Hz to 45 Hz. At each increment, the signal frequency was kept constant for 10 s. In figure 5, deformation from the spherical shape ζ is shown versus the drop oscillation frequency (f_D) along with photographs of typical patterns. ζ does not become zero since the drop was found to oscillate at any frequency of the applied signal. R_{max} was determined by measuring the diameter of a circle circumscribed around a deformed drop at maximum deformation, which was drawn onto a hard copy obtained from a video image. On the horizontal axis, the eigenfrequencies f_n obtained by linear theory (Rayleigh 1879) neglecting the effects of the surrounding fluid, that is the sulphuric acid, are also shown. The clear resonant oscillations of some modes are indicated by closed symbols while oscillations which do not show any clear mode, although having large deformation from the spherical shape, are indicated by open symbols. Patterns for $l = 2$, 3, 5 and 6 appeared clearly, but the pattern corresponding to $l = 4$ appeared only at one frequency. For other mercury drops of different radii, the fourth mode of oscillation was observed only in a very

https://doi.org/10.1017/S0022112099005728 Published online by Cambridge University Press

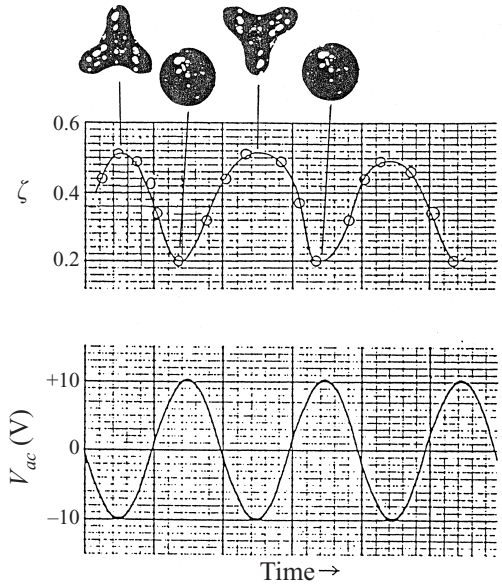


FIGURE 4. Relation of phases in the amplitude of the third-mode drop oscillation and the applied voltage. Frequency of the applied voltage is 5 Hz and the drop oscillation frequency is 2.5 Hz.

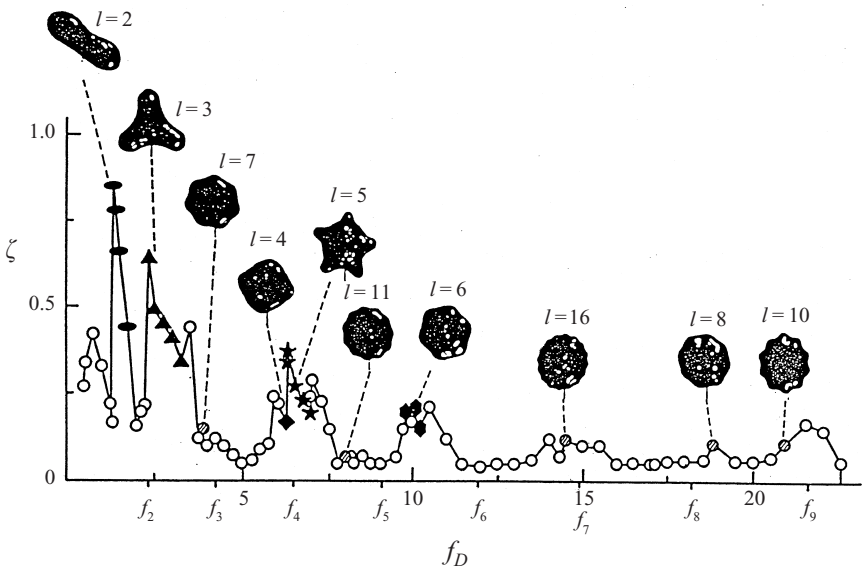


FIGURE 5. Deformation from the spherical shape ζ of the drop versus the frequency of oscillation f_D (Hz). Resonant frequencies f_l obtained by the linear theory are also shown. $R_0 = 1.05$ cm (13.6 g), $V_{ac} = \pm 10$ V.

narrow frequency band. The $l = 7$, 8, 10, 11 and 16 oscillation modes were excited, but at very different frequencies from those predicted by the linear theory. The seventh mode appeared between the third and the fourth and the eleventh mode appeared between the fifth and the sixth. Further, in the three-dimensional oscillations a strange mode appeared between the second and the third modes. These observations indicate interaction between waves.

https://doi.org/10.1017/S0022112099005728 Published online by Cambridge University Press

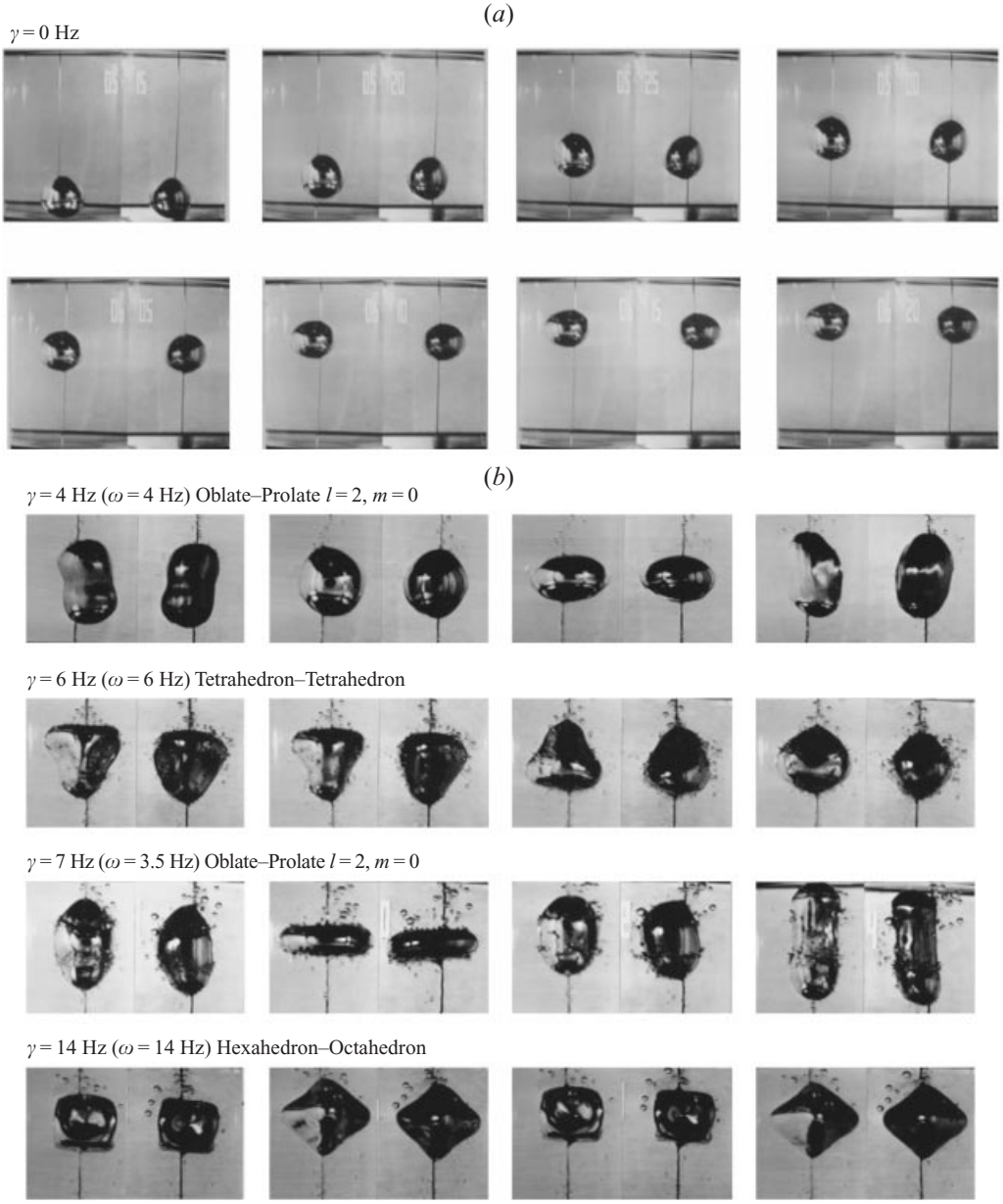


FIGURE 6 (*a*,*b*). For caption see page 318.

2.4. *Experimental results for three-dimensional oscillations under low-gravity conditions*

Three-dimensional large-amplitude drop oscillations in low gravity were obtained by varying the frequency of the applied signal in 1 Hz increments from 0 to 60 Hz, separate experimental runs being conducted for each fixed frequency. Images were taken with two video cameras every 1/30 s and successive pictures at 1/30 s intervals (1/15 s for the 2 Hz case) are shown in figures 6(*a*) to 6(*e*). The frequency of the alternating signal and the measured frequency of drop oscillations, in brackets, with the oscillation mode are shown for each sequence.

https://doi.org/10.1017/S0022112099005728 Published online by Cambridge University Press

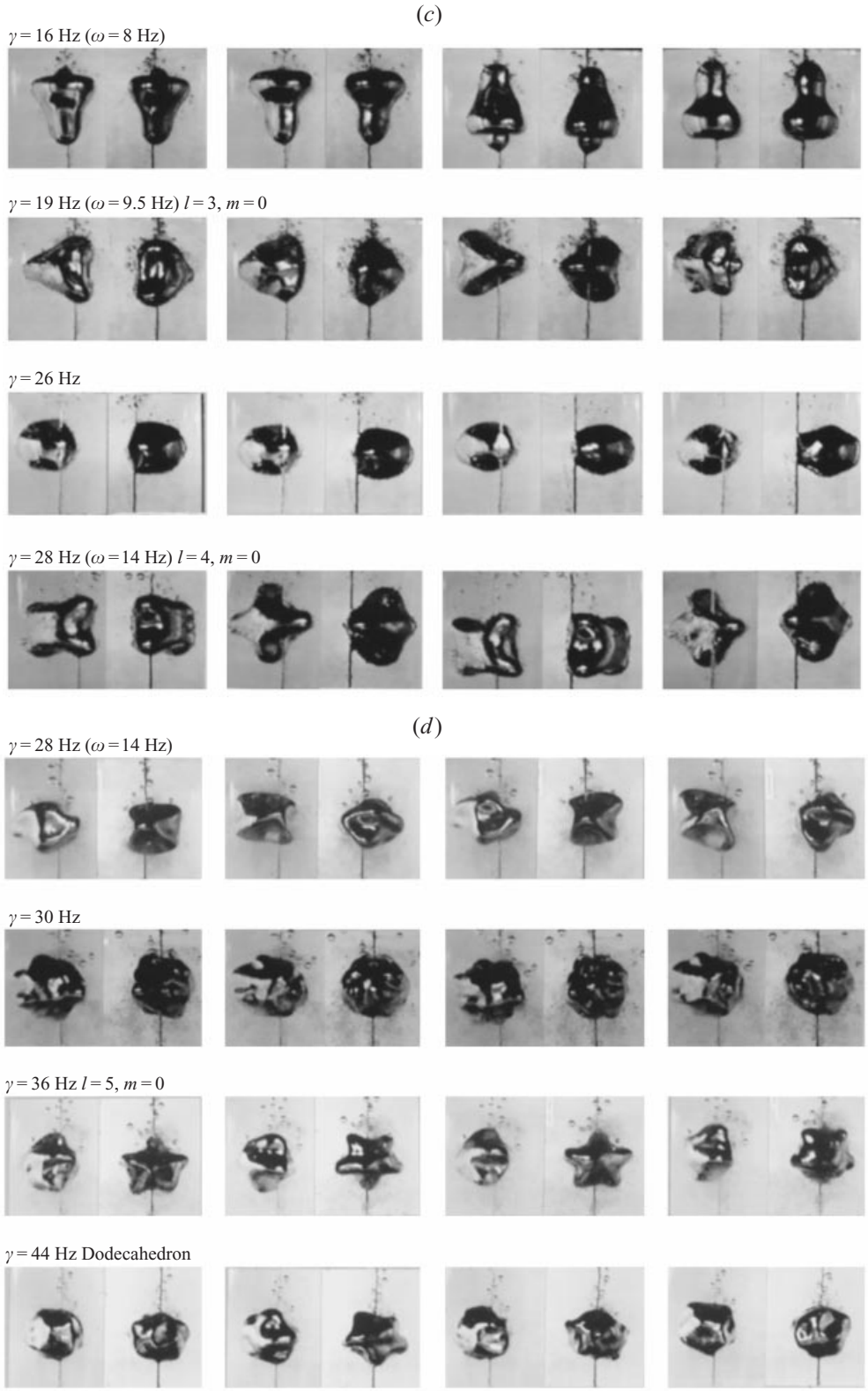


FIGURE 6 (*c*,*d*). For caption see page 318.

https://doi.org/10.1017/S0022112099005728 Published online by Cambridge University Press

(*e*)

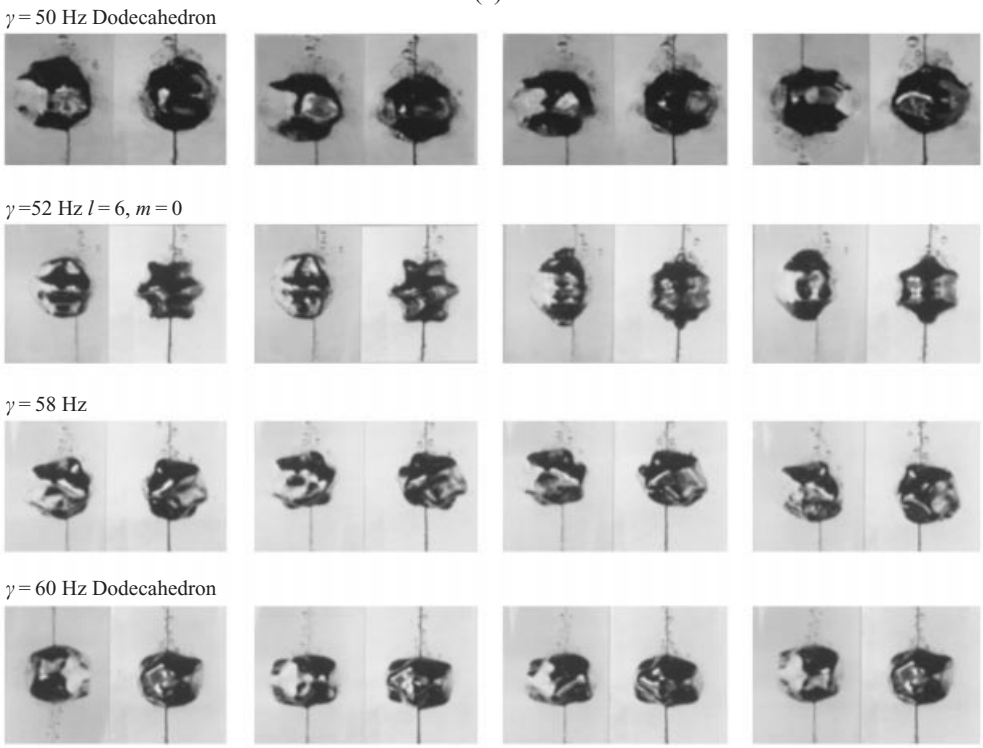


FIGURE 6. Photos of the variation of the three-dimensional oscillating patterns, taken every 1/30 s ($R_0 = 0.5$ cm). (*a*) $V_{ac} = \pm 0$ V, $f = 0$ Hz; (*b*, *c*) $V_{ac} = \pm 20$ V; (*d*, *e*) $V_{ac} = \pm 30$ V.

After the experiment capsule was released, the mercury drop moved upwards in its container accompanied by a small deflection of its surface (figure 6*a*), but this effect is thought to be negligible compared to the large-amplitude forced oscillation. Clear axisymmetric large-amplitude oscillations appeared only at the 4 Hz, 7 Hz ($l = 2$, $m = 0$) and 16 Hz ($l = 3$, $m = 0$) frequencies of the applied alternating signal; however, because there was no camera observing along the axis of the container this axisymmetry can only be supposed. For the 19, 28, 36 and 52 Hz cases, three-lobed, four-lobed, five-lobed and six-lobed modes appeared respectively. These oscillation patterns are inferred to be $m = 3$, $m = 4$, $m = 5$ and $m = 6$ modes at $l = 0$ respectively. The three-dimensional non-axisymmetric oscillation pattern ($l \neq 0$, $m \neq 0$) was also observed. A tetrahedron–tetrahedron oscillation was observed at 6 Hz, and a hexahedron–octahedron oscillation appeared at 14 Hz. At 44 Hz, a polyhedron based on a pentagon was observed, which is assumed to be a dodecahedron; a flat pentagon can be seen on its surface and the profile of the polyhedron is a pentagon. An oscillation pattern which is assumed to be sixth mode occurred around the 50 and 60 Hz frequencies; however, this is not clear due to the insufficient video frame rate. At 28 Hz, two oscillation patterns were observed, depending on the applied voltage (20 or 30 V). The first (at 20 V) is the oscillation mode of $l = 0$ and $m = 4$ and the second (at 30 V) is a twisted fourth mode. The signal voltage was raised from 20 V to 30 V from 28 Hz, because the higher voltage was necessary to obtain large amplitudes at higher frequency oscillations. The results indicate that the oscillation patterns change due to the applied external force magnitude, and the twisted pattern appeared at a higher energy than that of the four-lobed one.

https://doi.org/10.1017/S0022112099005728 Published online by Cambridge University Press

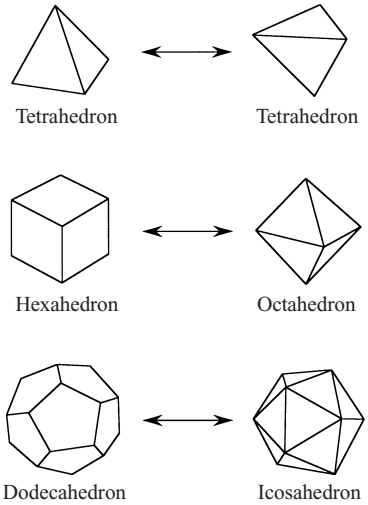


FIGURE 7. Polyhedra in duality relations.

The oscillation modes l and m were determined by comparing the shapes obtained in the experiments to those obtained by Arai *et al.* (1991) and also to the surface obtained by plotting the function using three-dimensional computer graphics,

$$r_s(\theta, \phi) = R[1 + aP_l^m(\cos\theta)e^{im\phi}],$$

where r_s is the radius of the deformed drop, R is the radius of the spherical non-deformed drop and a is the amplitude of oscillation.

These polyhedral oscillations occurred between polyhedra which are duals of each other. A facet of a polyhedron oscillates to produce a projection which forms, with other projections, a facet of another polyhedron. The dual relations among the Platonic polyhedra are shown in figure 7.

3. Theoretical analysis

3.1. *Lagrangian of the oscillating drop*

In order to analyse our experimental results, the method of deriving the equations of drop motion by applying the variational principle to the appropriate Lagrangian, following Natarajan & Brown (1986, 1987), was used with the assumption that the deformation of the drop from the original sphere is moderate. Irrotational inviscid flow was assumed for the drop motion due to its simplicity, but a dissipation term following the method of Lamb (1932, Art 355) was added. The effect of the surrounding fluid was neglected; this is assumed to be reasonable because the surrounding fluid is of much lower density than the mercury drop.

The analysis was simplified based on our experimental observations. Usually, periodic large-amplitude oscillations are caused by an external force and only one or a few harmonics waves are expected to occur, instead of the infinite number of low-amplitude waves of a wide range of frequencies which are usually considered in linear theory. Unrealistic waves can thus be neglected in the case of large-amplitude oscillations of the drop. In the same way, only some of the degenerate modes are thought to appear.

Present theory can deal with small- to moderate-amplitude drop oscillations of a low-viscosity liquid. Following the definition of Basaran (1992), the regions in which

https://doi.org/10.1017/S0022112099005728 Published online by Cambridge University Press

present theory is applicable are $A/L \ll 1$ and $\infty > \rho L^2/\mu t^* \gg 1$, where A/L is the amplitude-to-wavelength ratio and $\rho L^2/\mu t^*$ is the ratio of the time scale for vorticity to diffuse from the interface into the interior of the drop to the time scale for the fluid motion t^*. Although the latter region is applicable to mercury, the amplitudes of oscillations obtained in the experiments at low frequencies lie outside the former region.

As in Natarajan & Brown (1986, 1987), the following equations are considered:

$$r_s(\theta, \phi, t) = R[1 + \varepsilon\zeta(\theta, \phi, t)], \tag{3.1a}$$

$$\varphi(r, \theta, \phi, \xi) = (\sigma R/\rho)^{1/2}[\varepsilon\varphi'(\eta, \theta, \phi, t)], \tag{3.1b}$$

$$\bar{p}_0(t) = (\sigma/R)[-2 + \varepsilon^2 p_0'(t)], \tag{3.1c}$$

where the dimensionless radial coordinate η and the dimensionless time coordinate ξ are normalized as $\eta = r/R$ and $\xi = t/(\rho R^3/\sigma)^{1/2}$. If it is assumed that the deformation ζ of the radius of the drop from that of the spherical shape is sufficiently small, a special solution for the velocity potential is given by linear theory (Landau & Lifshitz 1958*b*) as

$$\varphi = A\mathrm{e}^{\mathrm{i}\omega\xi}\eta^{\ell} P_{\ell}^{m}(\cos\theta)\mathrm{e}^{\mathrm{i}m\phi} = A\mathrm{e}^{\mathrm{i}\omega\xi}\eta^{\ell} Y_{\ell}^{m}, \tag{3.2}$$

where $P_{\ell}^{m}(\cos\theta)\mathrm{e}^{\mathrm{i}m\phi}$ and Y_{ℓ}^{m} are the associated Legendre polynomials. From the kinematic condition $\partial\zeta/\partial t = \upsilon_r = \partial\varphi/\partial r$ at $r = 1$, the deformation is given as

$$\zeta = \frac{\ell}{\mathrm{i}\omega} Y_{\ell}^{m} A\mathrm{e}^{\mathrm{i}\omega\xi}. \tag{3.3}$$

The velocity potential and the deformation are expressed as general solutions:

$$\varphi = \sum \eta^{\ell} Y_{\ell}^{m}\mathrm{e}^{\mathrm{i}\omega\xi} \equiv \sum \eta^{\ell} R_{\ell}, \tag{3.4a}$$

$$\zeta = \sum \frac{\ell}{\mathrm{i}\omega} Y_{\ell}^{m}\mathrm{e}^{\mathrm{i}\omega\xi} = \sum \frac{\ell}{\mathrm{i}\omega} R_{\ell} \equiv \sum S_{\ell}, \tag{3.4b}$$

where R_{ℓ} and S_{ℓ} are time-dependent surface spherical harmonics of degree ℓ.

In the case of forced oscillations, it can be assumed that only one wave becomes dominant. Setting $\varphi = \eta^n R_n$ and $\zeta = S_n$ as first approximations is thought to be reasonable considering the experimental results. The dimensionless Lagrangian L' given by Natarajan & Brown (1987) then becomes

$$\begin{aligned} L' = {} & \varepsilon^2 \iint \left[\left(\tfrac{1}{2}n(n+1) - 1\right) S_n^2 + \tfrac{1}{2}nR_n^2 - \frac{\partial R_n}{\partial \xi} S_n \right] \sin\theta \,\mathrm{d}\theta \,\mathrm{d}\phi \\ & + \varepsilon^3 \iint \left[p_0' S_n - \tfrac{2}{3}S_n^3 + \tfrac{1}{4}n(3n+1)R_n^2 S_n - \tfrac{1}{2}(n+2)\frac{\partial R_n}{\partial \xi} S_n^2 \right] \sin\theta \,\mathrm{d}\theta \,\mathrm{d}\phi \\ & + \varepsilon^4 \iint \left[p_0' S_n^2 - \tfrac{1}{8} \left\{ n^2(n+1)^2_{c=0} \text{ or } \tfrac{1}{4}n^2(n+1)^2_{c=n} \text{ or } n^4_{c=2n} \right\} S_n^4 \right. \\ & \qquad + \left\{ \tfrac{1}{2}n^2(2n+1)_{c=0} \text{ or } \tfrac{1}{4}n^2(3n+1)_{c=n} \text{ or } 0_{c=2n} \right\} R_n^2 S_n^2 \\ & \qquad \left. - \tfrac{1}{6}(n+1)(n+2)\frac{\partial R_n}{\partial \xi} S_n^3 \right] \sin\theta \,\mathrm{d}\theta \,\mathrm{d}\phi, \end{aligned} \tag{3.5}$$

where $p_0' = \frac{2}{3}S_n^2$ from the conservation of mass at $O(\varepsilon^3)$. In the terms of $O(\varepsilon^4)$ of (3.5), three values, all of which depend on the value of c, are described as the coefficients

https://doi.org/10.1017/S0022112099005728 Published online by Cambridge University Press

of S_n^4 and $R_n^2 S_n^2$, as in the four-fold integrals (A5), (A6) and (A7) in Appendix A of Natarajan & Brown (1987).

When $n = 2$, for example, c takes the values 0, 2 and 4, and when $n = 3$, c takes the values 0, 2, 4 and 6. This is owing to the condition that the degrees of the spherical harmonics (a, b, c) must satisfy the relations $a + b + c = 2g$ (where g is an integer), $a \geqslant 0$, $b \geqslant 0$, and $|a - b| \leqslant c \leqslant a + b$ for the three-fold integrals of the spherical harmonics to be non-zero.

3.2. *Governing equations and variation of frequency as a function of amplitude*

Using the Lagrange equation

$$\frac{\mathrm{d}}{\mathrm{d}t}\left(\frac{\partial L'}{\partial \dot{q}}\right) - \frac{\partial L'}{\partial q} = 0, \tag{3.6}$$

the third-order kinetic equation is first obtained as

$$\frac{\omega_n^2}{\omega^2}\ddot{S}_n + \omega_n^2 S_n = \varepsilon\left\{-\frac{1}{2}(n+2)\frac{\partial^2}{\partial\xi^2}S_{n0}^2 - \frac{1}{4}n^2(3n+1)R_{n0}^2 + n(n+2)\frac{\partial R_{n0}}{\partial\xi}S_{n0} - \frac{\partial}{\partial\xi}\left[\frac{1}{2}n(3n+1)R_{n0}^2 S_{n0}\right]\right\} - \left(1 - \frac{\omega_n^2}{\omega^2}\right)\ddot{S}_n, \tag{3.7}$$

with

$$S_n = S_{n0} + \varepsilon S_{n1} \tag{3.8a}$$

and

$$S_{n0} = \bar{a}\cos\omega\xi, \quad \bar{a} \equiv \overline{S}_n(\theta, \phi), \tag{3.8b}$$

where $\bar{a}$ is the normalized maximum amplitude of the drop oscillation. To obtain the first-order derivation from the values of the linear theory:

$$\omega = \omega_n + \varepsilon\omega_{n1}, \tag{3.8c}$$

$$\omega_n^2 = n[n(n+1) - 2]; \tag{3.8d}$$

$$\left(1 - \frac{\omega_n^2}{\omega^2}\right)\ddot{S}_n = \frac{\varepsilon 2\omega_n\omega_{n1} + \varepsilon^2\omega_{n1}^2}{\omega^2}\bar{a}\omega^2(-\cos\omega t) \sim -\varepsilon 2\bar{a}\omega_n\omega_{n1}\cos\omega t. \tag{3.8e}$$

In (3.7), the term $(1 - \omega_n^2/\omega^2)\ddot{S}_n$ is subtracted from both sides for $S_{n0} = \bar{a}\cos\omega t$, which has the right frequency ω, to satisfy the left-hand side of (3.7) which is equal to zero.

The kinetic equation (3.7) is then transformed to

$$\frac{\omega_n^2}{\omega^2}\ddot{S}_{n1} + \omega_n^2 S_{n1} = 2\bar{a}\omega_{n1}\omega_n\cos\omega\xi + B\cos 2\omega\xi + C, \tag{3.9a}$$

with

$$B = \tfrac{1}{8}(21\bar{a}^2\omega^2 + 3\bar{a}^2 n\omega^2) \tag{3.9b}$$

and

$$C = \tfrac{1}{8}(7\bar{a}^2\omega^2 + \bar{a}^2 n\omega^2). \tag{3.9c}$$

From the condition that the secular term must disappear, we obtain $\omega_{n1} = 0$ and

https://doi.org/10.1017/S0022112099005728 Published online by Cambridge University Press

solutions

$$S_{n1} = -\frac{B}{3\omega_n^2}\cos 2\omega\xi + \frac{C}{\omega_n^2}, \tag{3.10a}$$

$$R_{n1} = -\frac{1}{n}\frac{2}{3}\frac{\omega}{\omega_n^2}B\sin 2\omega\xi. \tag{3.10b}$$

Next, proceeding to the second-order deviation with

$$S_n = S_{n0} + \varepsilon S_{n1} + \varepsilon^2 S_{n2} \tag{3.11a}$$

and

$$\omega = \omega_n + \varepsilon^2\omega_{n2} \tag{3.11b}$$

$$\left(1 - \frac{\omega_n^2}{\omega^2}\right)\ddot{S}_n = \frac{\varepsilon^2 2\omega_n\omega_{n2} + \varepsilon\omega_{n2}^2}{\omega^2}\bar{a}\omega^2(-\cos\omega t) \sim -\varepsilon^2 2\bar{a}\omega_n\omega_{n2}\cos\omega t, \tag{3.11c}$$

the fourth-order kinetic equation is obtained:

$$\begin{aligned}
\frac{\omega_n^2}{\omega^2}\ddot{S}_{n2} + \omega_n^2 S_{n2} = {} & -(n+2)\frac{\partial^2}{\partial\xi^2}(S_{n0}S_{n1}) - \tfrac{1}{6}(n+1)(n+2)\frac{\partial^2}{\partial\xi^2}(S_{n0}^3) \\
& -\tfrac{1}{2}n(3n+1)\frac{\partial}{\partial\xi}\{R_{n0}S_{n1} + R_{n1}S_{n0}\} \\
& -\left[n^2(2n+1)_{c=0} \text{ or } \tfrac{1}{2}n^2(3n+1)_{c=n} \text{ or } 0_{c=2n}\right]\frac{\partial}{\partial\xi}(R_0S_0^2) \\
& -\tfrac{1}{2}n^2(3n+1)R_{n0}R_{n1} + n(n+2)\left(\frac{\partial R_{n1}}{\partial\xi}S_{n0} + \frac{\partial R_{n0}}{\partial\xi}S_{n1}\right) \\
& -\tfrac{8}{3}nS_{n0}^3 + \tfrac{1}{2}\left[n^3(n+1)_{c=0}^2 \text{ or } \tfrac{1}{4}n^2(n+1)_{c=n}^2 \text{ or } n_{c=2n}^5\right]S_{n0}^3 \\
& -\left[n^3(2n+1)_{c=0} \text{ or } \tfrac{1}{2}n^3(3n+1)_{c=n} \text{ or } 0_{c=2n}\right]R_{n0}^2S_{n0} \\
& +\tfrac{1}{2}n(n+1)(n+2)\frac{\partial}{\partial\xi}R_{n0}S_{n0}^2 \\
& +2\bar{a}\,\omega_n\,\omega_{n2}\cos\omega\xi.
\end{aligned} \tag{3.12}$$

In the case of $n = 2$, there exist three coupling values $c = 0$, 2, 4 in the four-fold integral of S_2 and the values of the integral at each value of c are obtained from (A4)–(A8) of the Appendix as mentioned above. Considering the factor as $(2c + 1)$, the ratios of the values of the integrals with $(a = b = 2,\ \alpha = \beta = 0)$ corresponding to $c = 0,\ c = 2$ and $c = 4$ are $\frac{1}{5}$, $\frac{1}{7}$ and $\frac{3}{70}$. From the principle that the Lagrangian (3.5) should take a minimum value in a physical process, it is thought that a coupling at $c = 0$ probably occurs.

The condition that the coefficient of $\cos\omega\xi$ must disappear when $c = 0$ yields

$$\omega_{n2} = \bar{a}^2\left\{\frac{1}{\omega_n}\left(n - \frac{3n^3}{16} - \frac{3n^4}{8} - \frac{3n^5}{16}\right) + \omega_n\left(\frac{17}{64} - \frac{9n}{32} + \frac{17n^2}{64}\right)\right\} = k\bar{a}^2, \tag{3.13}$$

with

$$\omega_{22} = -1.90\bar{a}^2 \quad \text{at} \quad n = 2 \tag{3.14}$$

https://doi.org/10.1017/S0022112099005728 Published online by Cambridge University Press

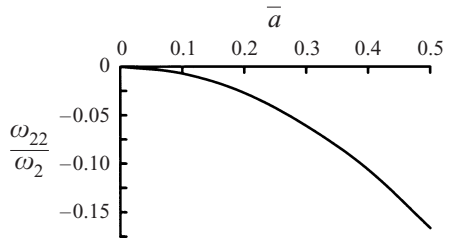


FIGURE 8. The ratio of the frequency decrease ω_{22}/ω_2 versus the amplitude of oscillation $\bar{a}$ (for $c = 0$).

and

$$\omega_{32} = -4.31\bar{a}^2 \quad \text{at} \quad n = 3. \tag{3.15}$$

The ratio of the frequencies $|\omega_{22}/\omega_2|$ increases with increasing amplitude of oscillation, as shown in figure 8.

3.3. *Amplitude of drop oscillations caused by an external force*

3.3.1. *Dissipation of the oscillating drop*

If the velocity potential has the following form:

$$\phi = \frac{r^n}{R^n} R'_n = \eta^n R'_n, \tag{3.16}$$

the total dissipation of the oscillating drop is given by Lamb (1932, Art 355) as

$$J = 2F = 2n(n-1)(2n+1)\frac{\mu}{R}\int_0^{2\pi}\int_0^{\pi} R_n'^2 \sin\theta \, \mathrm{d}\theta \, \mathrm{d}\phi. \tag{3.17}$$

The total dissipation J is normalized to correspond to (3.5) by the following transformation:

$$R \to 1, \tag{3.18a}$$

$$\phi = (\sigma R/\rho)^{1/2}[\varepsilon\phi'(\eta, \theta, \phi, \xi)] = (\sigma R/\rho)^{1/2}\varepsilon\eta^n R_n(\theta, \phi, \xi), \tag{3.18b}$$

$$\mu' = \frac{\mu}{(\rho R^3/\sigma)^{1/2}}, \quad R_n = -\frac{1}{n}\frac{\partial S_n}{\partial \xi}, \quad v' = \frac{v}{(\rho R^3/\sigma)^{1/2}}. \tag{3.18c}$$

Normalized total dissipation J', corresponding to (3.5), is expressed, considering the increase of the drop surface δA by deformation effects

$$1 + \delta A = 1 + 2\zeta\varepsilon + \varepsilon^2\left[\zeta^2 + \tfrac{1}{2}(\zeta_\theta^2 + \zeta_\phi^2 \operatorname{cosec}^2\theta)\right] + \varepsilon^3(0),$$

by

$$J' = \frac{2(n-1)(2n+1)}{n} v' \int_0^{2\pi}\int_0^{\pi}\left(\frac{\partial S_n}{\partial x}\right)^2 (1 + 2S_n + \cdots)\sin\theta \, \mathrm{d}\theta \, \mathrm{d}\phi \tag{3.19}$$

and the term to be added to the Lagrange equation is

$$\frac{\partial J'}{\partial \dot{S}_n} = v' \frac{4(n-1)(2n+1)}{n} \int_0^{2\pi}\int_0^{\pi}\left(\frac{\partial S_n}{\partial x}\right)(1 + 2S_n + \cdots)\sin\theta \, \mathrm{d}\theta \, \mathrm{d}\phi \tag{3.20}$$

https://doi.org/10.1017/S0022112099005728 Published online by Cambridge University Press

as

$$\frac{\mathrm{d}}{\mathrm{d}t}\left(\frac{\partial L'}{\partial \dot{q}}\right) - \frac{\partial L'}{\partial q} + \frac{\partial J'}{\partial \dot{q}} = 0. \tag{3.21}$$

Here, the damping coefficient is normalized as

$$\lambda' = \frac{4(n-1)(2n+1)}{n} v'. \tag{3.22}$$

3.3.2. *Forced oscillation equation*

An oscillating surface tension $\sigma_0(1 + f\mathrm{e}^{\mathrm{i}\gamma\xi})$ is considered as an external force term. The terms associated with surface tension in the Lagrangian (as in (4) of Natarajan & Brown 1986) are expressed as

$$\iint \sigma_0(1+f\mathrm{e}^{\mathrm{i}\gamma\xi}) r_s^2 \left(1 + \frac{r_\theta^2}{r_s^2} + \frac{r_\phi^2}{r^2}\operatorname{cosec}^2\theta\right)^{1/2} r_s \sin\theta \,\mathrm{d}\theta \,\mathrm{d}\phi = \iint \sigma_0(1+f\mathrm{e}^{\mathrm{i}\gamma\xi}) R^2$$
$$\times\left\{1 + 2\zeta\varepsilon + \varepsilon^2\left[\zeta^2 + \tfrac{1}{2}(\zeta_\theta^2 + \zeta_\phi^2 \operatorname{cosec}^2\theta)\right] + O(\varepsilon^3) + \cdots\right\} r_s \sin\theta \,\mathrm{d}\theta \,\mathrm{d}\phi \tag{3.23a}$$

with the contribution of the third term as

$$\iint \sigma_0(1+f\mathrm{e}^{\mathrm{i}\gamma\xi})/R[-2 + \varepsilon^2 p_0'] \left[\tfrac{1}{3}R^3(1+\varepsilon\zeta)^3 - \tfrac{1}{4\pi}V\right] \sin\theta \,\mathrm{d}\theta \,\mathrm{d}\phi. \tag{3.23b}$$

Then, the terms in the dimensionless Lagrangian associated with the surface tension L'_{f0} and the Lagrange equation to the second order become respectively

$$L'_{f0} = f\mathrm{e}^{\mathrm{i}\gamma\xi}\left\{1 + 2\varepsilon S_n + \varepsilon^2\left[\tfrac{1}{2}n(n+1)S_n^2\right]\right\}, \tag{3.24a}$$

$$\frac{\partial L'_{f0}}{\partial S_n} = f\mathrm{e}^{\mathrm{i}\gamma\xi}\varepsilon^2 n(n+1) S_n. \tag{3.24b}$$

From (3.23), it can be deduced that the variation of the surface tension is equal to the variation of the pressure. That suggests that (3.23) are applicable to acoustic oscillations. The kinetic equation (3.7) is expressed, including the damping term, as follows:

$$\ddot{S}_n + 2\lambda'(1+2S_n)\dot{S}_n + \omega_n^2(1 + h\cos\gamma\xi)S_n = \varepsilon\{\text{NL terms}\}, \tag{3.25a}$$

$$h = n^2(n+1)f/\omega_n^2 \tag{3.25b}$$

with

$$\lambda = \lambda'(1+2S_n). \tag{3.26}$$

Equation (3.25*a*) becomes the Mathieu equation, regarding λ as the apparent damping coefficient:

$$\ddot{S}_n + 2\lambda\dot{S}_n + \omega_n^2(1 + h\cos\gamma\xi)S_n = \varepsilon\{\text{NL terms}\}. \tag{3.27}$$

It is known from the experimental result shown in figure 4 that the strongest resonance occurs when γ is nearly twice ω_n. From setting $\gamma = 2\omega_n + \varepsilon$ and looking for $S_n = \bar{a}\cos\left[\left(\omega_n + \frac{1}{2}\varepsilon\right)\xi + \delta\right]$, the resultant equation of the forced oscillation is obtained as

$$\ddot{S}_n + 2\lambda\dot{S}_n + \omega_n^2 S_n = -\tfrac{1}{2}n^2(n+1)f\bar{a}\cos\left[\left(\omega_n + \tfrac{1}{2}\varepsilon\right)\xi - \delta\right] + \varepsilon\{\text{NL terms}\}. \tag{3.28}$$

https://doi.org/10.1017/S0022112099005728 Published online by Cambridge University Press

$n=2$	R (cm)	f_k	$n=3$	R (cm)	f_k
	1	0.054		1	0.098
	0.5	0.15		0.5	0.28
	0.25	0.43		0.25	0.79
	0.1	1.72		0.1	3.11

TABLE 2. Threshold of f for various drop radii.

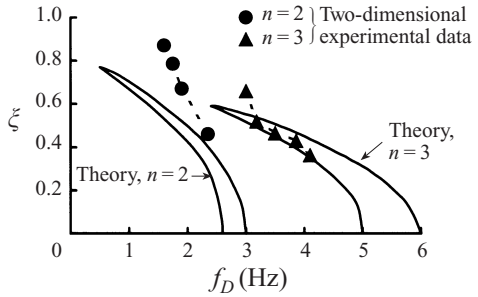


FIGURE 9. The amplitude versus the frequency of the forced oscillation. (Experimental data are two-dimensional and are from figure 5, $n=2$, $R=1$ cm, $f=0.11$, $k=1.90\,(c=0)$ and $n=3$, $R=1$ cm, $f=0.18$, $k=-4.31\,(c=0)$.)

From (3.28), the values of the amplitude of oscillation $\bar{a}$ are obtained, following Landau & Lifshitz (1958*a*), as follows:

$$\bar{a}=0, \tag{3.29a}$$

$$\bar{a}^2=\frac{1}{k}\left[\frac{\varepsilon}{2}+\sqrt{\left(\frac{1}{16\omega_n^2}n^4(n+1)^2f^2\right)-\lambda^2}\right], \tag{3.29b}$$

$$\bar{a}^2=\frac{1}{k}\left[\frac{\varepsilon}{2}-\sqrt{\left(\frac{1}{16\omega_n^2}n^4(n+1)^2f^2\right)-\lambda^2}\right]. \tag{3.29c}$$

As λ can be approximated as

$$\lambda=\lambda'(1+2\bar{a}),$$

the amplitude $\bar{a}$ versus ε is obtained from (3.29).

The threshold of f which causes the strong resonance, obtained from $h_k=4\lambda/\omega_n$, is shown in table 2.

In the case of a mercury sphere ($\nu=0.0012\,\mathrm{cm^2\,s^{-1}}$, $\sigma=300\,\mathrm{dyne\,cm^{-1}}$, $\rho=13\,\mathrm{g\,cm^{-3}}$), the theoretical variation of the amplitude of oscillation as a function of frequency in the case $c=0$ is shown in figure 9 for $f=0.11\,(n=2)$ and 0.18 ($n=3$), along with the experimental results ($n=2$ and $n=3$) of the two-dimensional case, which are also shown in figure 5. Both results can be seen to be in fairly good agreement with the theory when the drop deformation is moderate ($\zeta<0.5$). However, there is a large discrepancy between theoretical predication and experimental result when the deformation is very large ($\zeta>0.5$). This indicates the limitations of the present analysis. Comparison between theoretical predictions and experimental results for the cases $c=0$, 2 and 4 shows that the prediction in the case $c=0$ is in closest agreement with the results, especially at the $n=3$ mode. This fact indicates that the

https://doi.org/10.1017/S0022112099005728 Published online by Cambridge University Press

choice of $c = 0$ in (3.12) is reasonable. In the prediction, a larger value of f for $n = 3$ than that of the experiment ($f = 0.11$) was used. This comes from the fact that the experimental result is for a quasi-two-dimensional oscillation; that is, the increase in the drop surface area, included in the damping term of (3.25*a*), is smaller in a two-dimensional oscillation than in a three-dimensional one.

4. Discussion

An explanation can be given concerning the reason for the appearance of tetra–tetrahedron oscillations as cubic nonlinearities, hexa–octahedron oscillations as quadratic nonlinearities and dodecahedron–icosahedron oscillations near the main resonance, although the mathematics lacks rigour. The experimental results shown in figure 6 indicate that multi-lobed oscillations ($l = 0$) occur at the main resonance, at $\gamma = 2\omega_n + \varepsilon$. Also, the oscillation between polyhedra (fifth and sixth modes) occurs at nearly the same frequency as that of the multi-lobed oscillation ($l = 0$, $m = 5$ and 6). The reason is thought to be as follows. In the dimensionless Lagrangian (3.7), quadratic terms of S_n are given by

$$L' = \cdots \varepsilon^2 \iint S_6 S_6 \sin\theta \,\mathrm{d}\theta \,\mathrm{d}\phi$$

$$= \cdots \varepsilon^2 \iint C_6^6 C_6^{-6} \exp\left(2\mathrm{i}\left\{\left(\omega_n + \frac{\varepsilon}{2}\right)\xi - \delta\right\}\right) \sin\theta \,\mathrm{d}\theta \,\mathrm{d}\phi \tag{4.1a}$$

or, equivalently, by

$$\varepsilon^2 \iint C_6^0 C_6^0 \exp\left(2\mathrm{i}\left\{\left(\omega_n + \frac{\varepsilon}{2}\right)\xi - \delta\right\}\right) \sin\theta \,\mathrm{d}\theta \,\mathrm{d}\phi. \tag{4.1b}$$

Equation (A3) of the Appendix shows that the values of the above integrals depend only on the value of a (6 in this case) and are equal. The corresponding term in the kinetic equation becomes

$$\frac{\partial L'}{\partial S_6} = \cdots \varepsilon^2 \iint C_6^6 \exp\left(\mathrm{i}\left\{\left(\omega_n + \frac{\varepsilon}{2}\right)\xi - \delta\right\}\right) \sin\theta \,\mathrm{d}\theta \,\mathrm{d}\phi \tag{4.2a}$$

or

$$\varepsilon^2 \iint C_6^6 \exp\left(\mathrm{i}\left\{\left(\omega_n + \frac{\varepsilon}{2}\right)\xi - \delta\right\}\right) \sin\theta \,\mathrm{d}\theta \,\mathrm{d}\phi. \tag{4.2b}$$

From this, both axisymmetric ($l = n$, $m = 0$) and non-axisymmetric ($l = n$, $m = n$) modes which occur from the main resonance have the same frequency.

At $\gamma = \omega_n + \frac{1}{2}\varepsilon$, the oscillation between a hexahedron and an octahedron ($l = 4$) occurred at about half the frequency of the axisymmetric oscillation ($l = 4$, $m = 0$), which suggests that this oscillation is caused by the quadratic nonlinearities in the right-hand side of the kinetic equation (3.7). In the dimensionless Lagrangian (1.7), the cubic term must be

$$L' = \cdots \varepsilon^3 \iint S_4 S_4 S_4 \sin\theta \,\mathrm{d}\theta \,\mathrm{d}\phi$$

$$= \cdots \varepsilon^3 \iint C_4^4 C_4^{-4} C_4^0 \exp\left(3\mathrm{i}\left\{\left(\frac{\omega_n}{2} + \frac{\varepsilon}{4}\right)\xi - \delta\right\}\right) \sin\theta \,\mathrm{d}\theta \,\mathrm{d}\phi \tag{4.3}$$

https://doi.org/10.1017/S0022112099005728 Published online by Cambridge University Press

because $\alpha + \beta + \gamma = 0$ must be satisfied. The corresponding term of the kinetic equation becomes

$$\frac{\partial L'}{\partial S_4} = \cdots \varepsilon^3 \iint S_4 S_4 \sin\theta \,\mathrm{d}\theta \,\mathrm{d}\phi$$

$$= \cdots \varepsilon^3 \iint C_4^4 C_4^{-4} \exp\left(2\mathrm{i}\left\{\left(\frac{\omega_n}{2} + \frac{\varepsilon}{4}\right)\xi - \delta\right\}\right) \sin\theta \,\mathrm{d}\theta \,\mathrm{d}\phi. \tag{4.4}$$

Here, a differentiation was conducted with regard to S_4 of $m = 0$.

At $\gamma = \frac{2}{3}\omega_n + \frac{1}{3}\varepsilon$, the oscillation between a tetrahedron and a tetrahedron occurred at about one third of the frequency of the axisymmetric oscillation ($l = 3,\ m = 0$). This oscillation is thought to be caused by the cubic nonlinearities of the kinetic equation (3.12). The fourth-order term

$$L' = \cdots \varepsilon^4 \iint S_3 S_3 S_3 S_3 \sin\theta \,\mathrm{d}\theta \,\mathrm{d}\phi$$

$$= \cdots \varepsilon^4 \iint C_3^3 C_3^{-3} C_3^0 C_3^0 \exp\left(4\mathrm{i}\left\{\left(\frac{\omega_n}{3} + \frac{\varepsilon}{6}\right)\xi - \delta\right\}\right) \sin\theta \,\mathrm{d}\theta \,\mathrm{d}\phi \tag{4.5}$$

produces the cubic term:

$$\frac{\partial L'}{\partial S_3} = \cdots \varepsilon^4 \iint S_3 S_3 S_3 \sin\theta \,\mathrm{d}\theta \,\mathrm{d}\phi$$

$$= \cdots \varepsilon^4 \iint C_3^3 C_3^{-3} C_3^0 \exp\left(3\mathrm{i}\left\{\left(\frac{\omega_n}{3} + \frac{\varepsilon}{6}\right)\xi - \delta\right\}\right) \sin\theta \,\mathrm{d}\theta \,\mathrm{d}\phi. \tag{4.6}$$

The differentiation was also conducted for S_3 of $m = 0$.

Considering that a term of higher-order nonlinearities has smaller energy than a term of lower-order nonlinearities and that for a higher-order oscillation mode, more energy is required to cause large-amplitude oscillation than for a lower oscillation mode, a weak externally forced oscillation is thought to cause the polyhedron oscillation. This is why at the fifth and sixth modes, polyhedron oscillations and multi-lobed oscillations coexist.

In figure 10, the frequencies of the drop oscillations obtained in the experiment are shown and compared with the values predicted by the linear theory. For the polyhedral oscillations, the tetrahedron is classified as the third mode, the hexahedron as the fourth and the dodecahedron as the fifth. At the vertical bars at the fifth and sixth modes, multi-lobed mode ($l = 0,\ m = 5, 6$) oscillations and polyhedron mode oscillations coexist.

Considering (3.23), $2\lambda'(1 + 2S_n)$, the dissipation term, becomes negative for a small period of a cycle when the amplitude of oscillation is larger than 0.5. At that time, energy is absorbed into the oscillation. This may be the reason why the maximum amplitudes of oscillation, at half-cycle different phases, are different.

5. Conclusions

Two- and three-dimensional large-amplitude drop oscillations were obtained using a new method under both 1 g and low-gravity conditions. The frequency of drop oscillation was arbitrarily changed and the relationship between drop oscillation modes and frequencies was obtained. Various modes of drop oscillation have also been

https://doi.org/10.1017/S0022112099005728 Published online by Cambridge University Press

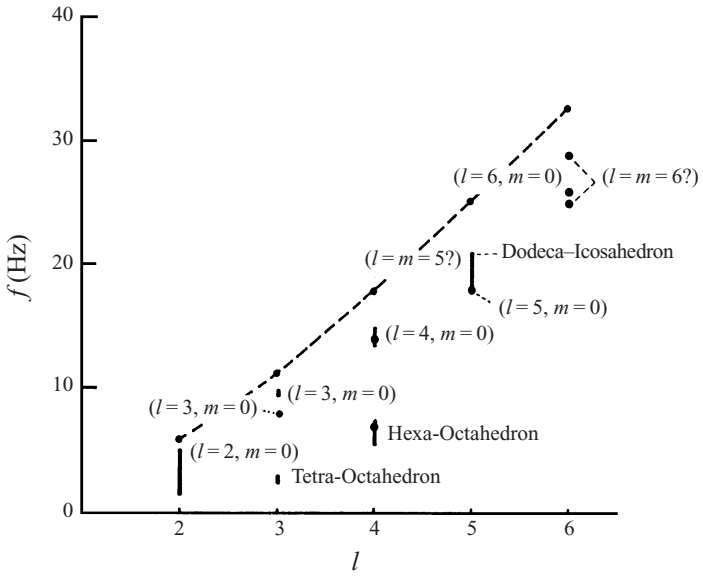


FIGURE 10. The relation between the three-dimensional oscillation modes and the frequency of the applied alternating voltage, at their occurrence. The linear theory values, calculated with $\sigma_{av} = 300\,\mathrm{dyne\,cm^{-1}}$, are also shown as a dashed line $R_0 = 0.5\,\mathrm{cm}$.

observed for the first time, and the nonlinear effects of waves coupling with the oscillation pattern is clearly shown. Some three-dimensional oscillation modes were found to be excited as subharmonics. Tetra–tetrahedron oscillation (third mode) occurred at one third of the frequency predicted by the linear theory and hexa–octahedron (fourth mode) oscillation at half the predicted frequency. However, polyhedral oscillations (fifth mode and sixth mode) were excited near the main resonant frequencies. Strange oscillation patterns, assumed to be a combination of two modes, were also excited.

Kinetic equations for the three-dimensional oscillating drop were derived by applying variational principles to the Lagrangian of the fourth-order of nonlinearity. A decrease of the first eigenfrequency from that predicted by linear analysis, due to finite-amplitude oscillation, was discovered. This decrease is proportional to the square of the amplitude of oscillation and depends on the degree of the spherical harmonics which are coupled in the fourth-order integral.

The governing equation for the forced oscillation of the drop was found to be a deformed nonlinear Mathieu equation. By deriving its solution, the relationships between oscillation mode, oscillation amplitude, external force, damping coefficient and frequency were obtained and compared with experimental results. These showed fairly good agreement, proving the correctness of the analysis. The appearance of polyhedra was explained using third- and fourth-order integrals of spherical harmonics. The relationship between the selection of an oscillation mode and a given energy was formulated by using integral values of quadratic, cubic and fourth-order nonlinear terms.

The authors acknowledge the referees for their helpful comments.

https://doi.org/10.1017/S0022112099005728 Published online by Cambridge University Press

Nomenclature

$\bar{a}$:	Normalized maximum amplitude of the drop oscillation
a, b, c, k, ℓ, m, n:	Degrees of the spherical harmonics
C_a^α:	Basis functions for spherical functions
f_D:	Frequency of drop oscillation
f_n:	Eigenfrequency of drop oscillation of mode n
f:	Variation ratio of the surface tension with respect to its average value
f_k:	Threshold of f to cause resonance
g:	Integer
J:	Total dissipation of the oscillating drop
J':	Dimensionless total dissipation
L:	The Lagrangian for an oscillating drop
L':	Dimensionless Lagrangian
L'_{f0}:	Dimensionless Lagrangian associated with surface tension variation
P_l:	The Legendre polynomials
P_a^α, P_ℓ^m:	Associated Legendre polynomials
$\bar{p}_0$:	The Lagrange multiplier corresponding to the pressure
p'_0:	Deviation of the pressure from the value corresponding to the static spherical drop
q:	A general coordinate
$\dot{q}$:	A general velocity
R:	Radius of a spherical drop
R_n:	Time-dependent surface spherical harmonics of degree n which correspond to the velocity potential
R_{n0}, R_{n1}, R_{n2}:	Surface spherical harmonics as solutions of the kinetic equation of the drop oscillation
R'_n:	Surface spherical harmonics which correspond to the velocity potential
r:	Coordinate in the radial direction
r_s:	Radius of the deformed drop
$r_\theta, r_\phi, r_{s\theta}, r_{s\phi}$:	Derivatives of r and r_s, with respect to θ and ϕ
S_n:	Surface spherical harmonics corresponding to the deviations from the spherical shape
S_{n0}, S_{n1}, S_{n2}:	Surface spherical harmonics as solutions of the kinetic equation of the drop oscillation
$\overline{S}_n$:	Time-independent part of the spherical harmonics S_n
S_m, S_ℓ, S_k:	Time-dependent surface spherical harmonics corresponding to the deviations from the spherical shape
t:	Time
Y_ℓ^m:	Associated Legendre polynomials
V:	Volume of the drop
α, β, γ:	Rank of the spherical harmonics
ρ:	Density of the liquid
$\varphi_r, \varphi_\theta, \varphi_\phi, \varphi_t, \varphi_\eta, \varphi_\xi$:	Derivatives of the velocity potential

https://doi.org/10.1017/S0022112099005728 Published online by Cambridge University Press

ε: Order of the amplitude of the drop oscillation or deviation of the frequency
ξ: Dimensionless time coordinate
η: Dimensionless radial coordinate
v_r: Velocity in the radial direction
ω: Frequency of the drop oscillation
ω_n: Eigenfrequency of the n linear drop oscillation mode
ω_{n1}, ω_{n2}: Deviation of the frequency of oscillation
μ: Viscosity coefficient
μ': Dimensionless viscosity coefficient
ν: Dynamic viscosity coefficient
ν': Dimensionless dynamic viscosity coefficient
σ, σ_0: Surface tension of the liquid
λ: Apparent damping coefficient
λ': Dimensionless damping coefficient
ζ: Maximum deformation from the spherical shape or amplitude of the drop oscillation
ζ_θ, ζ_ϕ: Derivatives of ζ with respect to θ and ϕ
$\delta_{ab}, \delta_{\alpha\beta}$: The Kronecker delta function
Θ: Normalized associated Legendre polynomial
k: Coefficient of the square of the amplitude expressing the decrease in the frequency
γ: Frequency of the external force

Appendix

Using the basis functions for the spherical harmonics, defined by Brink & Satchler (1968), the integrals of the product of two, three and four spherical-harmonic basis functions are given by (Natarajan & Brown 1987)

$$C_a^\alpha(\theta,\varphi) = (-1)^\alpha \left[\frac{(a-\alpha)!}{(a+\alpha)!}\right]^{1/2} P_a^\alpha(\theta)\mathrm{e}^{\mathrm{i}\alpha\varphi} \quad \text{if} \quad \alpha \geqslant 0, \tag{A 1}$$

$$C_a^{-\alpha}(\theta,\varphi) = (-1)^\alpha C_a^\alpha(\theta,\varphi)^*, \tag{A 2}$$

$$\int_0^{2\pi}\int_0^{\pi} C_a^\alpha(\theta,\varphi)C_b^\beta(\theta,\varphi)^* \sin\theta \,\mathrm{d}\theta \,\mathrm{d}\varphi = \frac{4\pi}{(2a+1)}\delta_{ab}\delta_{\alpha\beta}. \tag{A 3}$$

The integral of the product of three spherical harmonics is given in terms of the 3-j symbols and the Gaunt integral (Yoshida *et al.* 1967):

$$\int_0^{2\pi}\int_0^{\pi} C_a^\alpha C_b^\beta C_c^\gamma \sin\theta \,\mathrm{d}\theta \,\mathrm{d}\varphi = 4\pi \begin{pmatrix} a & b & c \\ 0 & 0 & 0 \end{pmatrix} \begin{pmatrix} a & b & c \\ \alpha & \beta & \gamma \end{pmatrix}$$

$$= \frac{(-1)^{g-a-\beta}(g-b)!g!}{(g-a)!(g-b)!(g-c)!(2g+1)!} \sqrt{\frac{(c-\alpha-\beta)!(a+\alpha)!(b+\beta)!(b-\beta)!}{(c+\alpha+\beta)!(a-\alpha)!}}$$

$$\times \sum_t (-)^t \frac{(c+\alpha+\beta+t)!(a+b-\alpha-\beta-t)!}{(c-\alpha-\beta-t)!(a-b+\alpha+\beta+t)!(b-\beta-t)!t!}, \tag{A 4}$$

https://doi.org/10.1017/S0022112099005728 Published online by Cambridge University Press

$$\int_0^{2\pi}\int_0^{\pi} C_a^{\alpha}C_b^{\beta}C_d^{\delta}C_e^{\varepsilon}\sin\theta\,\mathrm{d}\theta\,\mathrm{d}\varphi = \sum_{c=0}^{\min(a+b,c+d)}\int_0^{2\pi}\int_0^{\pi} C_a^{\alpha}C_b^{\beta}|_c C_d^{\delta}C_e^{\varepsilon}\sin\theta\,\mathrm{d}\theta\,\mathrm{d}\varphi$$

$$= \sum_{c=0}\phi^{(abde)}_{c;\alpha\beta\delta\varepsilon} \tag{A 5}$$

$$\phi^{(abde)}_{c;\alpha\beta\delta\varepsilon} = (-1)^{\alpha+\beta}(2c+1)\begin{pmatrix} a & b & c \\ 0 & 0 & 0 \end{pmatrix}\begin{pmatrix} a & b & c \\ \alpha & \beta & -\alpha-\beta \end{pmatrix} \times \begin{pmatrix} d & e & c \\ 0 & 0 & 0 \end{pmatrix}\begin{pmatrix} d & e & c \\ \delta & \varepsilon & \alpha+\beta \end{pmatrix}. \tag{A 6}$$

Then we have:

$$\iint S_aS_b|_cS_dS_e\sin\theta\,\mathrm{d}\theta\,\mathrm{d}\varphi$$

$$= \frac{a}{\mathrm{i}\omega}\left[\frac{(a+\alpha)!}{(a-\alpha)!}\right]^{1/2}(-1)^{\alpha}\frac{b}{\mathrm{i}\omega}\left[\frac{(b+\beta)!}{(b-\beta)!}\right]^{1/2}(-1)^{\beta}\frac{d}{\mathrm{i}\omega}\left[\frac{(d+\delta)!}{(d-\delta)!}\right]^{1/2}(-1)^{\delta} \times\frac{e}{\mathrm{i}\omega}\left[\frac{(e+\varepsilon)!}{(e-\varepsilon)!}\right]^{1/2}(-1)^{\varepsilon}\iint C_a^{\alpha}C_b^{\beta}|_cC_d^{\delta}C_e^{\varepsilon}\sin\theta\,\mathrm{d}\theta\,\mathrm{d}y \tag{A 7}$$

$$= \frac{a}{\mathrm{i}\omega}\left[\frac{(a+\alpha)!}{(a-\alpha)!}\right]^{1/2}(-1)^{\alpha}\frac{b}{\mathrm{i}\omega}\left[\frac{(b+\beta)!}{(b-\beta)!}\right]^{1/2}(-1)^{\beta}\frac{d}{\mathrm{i}\omega}\left[\frac{(d+\delta)!}{(d-\delta)!}\right]^{1/2}(-1)^{\delta}\frac{e}{\mathrm{i}\omega} \times\left[\frac{(e+\varepsilon)!}{(e-\varepsilon)!}\right]^{1/2}(-1)^{\varepsilon}(-1)^{\alpha+\beta}(2c+1)\begin{pmatrix} a & b & c \\ 0 & 0 & 0 \end{pmatrix}\begin{pmatrix} a & b & c \\ \alpha & \beta & -\alpha-\beta \end{pmatrix} \times\begin{pmatrix} d & e & c \\ 0 & 0 & 0 \end{pmatrix}\begin{pmatrix} d & e & c \\ \delta & \varepsilon & \alpha+\beta \end{pmatrix}. \tag{A 8}$$

REFERENCES

Arai, Y., Adachi, K. & Takaki, R. 1991 Spherical harmonic functions for expression of polyhedral vibration of a spherical drop. *Forma* **6**, 193–204.

Basaran, O. A. 1992 Nonlinear oscillations of viscous liquid drops. *J. Fluid Mech.* **241**, 169–198.

Becker, E., Hiller, W. J. & Kowalewski, T. A. 1991 Experimental and theoretical investigation of large-amplitude oscillations of liquid droplets. *J. Fluid Mech.* **231**, 189–210.

Becker, E., Hiller, W. J. & Kowalewski, T. A. 1994 Nonlinear dynamics of viscous droplets. *J. Fluid Mech.* **258**, 191–216.

Brink, D. M. & Satchler, G. M. 1968 *Angular Momentum*, 2nd Edn. Clarendon.

Egry, I., Lohoefer, G. & Sauerland, S. 1993 Measurement of thermophysical properties of liquid metals by noncontact techniques. *J. Thermophys.* **14**, 573–584.

Feng, J. Q. & Beard, K. V. 1991 Three-dimensional oscillation characteristics of electrostatically deformed drops. *J. Fluid Mech.* **227**, 429–447.

Lamb, H. 1932 *Hydrodynamics* (Art 355), 6th Edn. Cambridge University Press.

Landau, L. D. & Lifshitz, E. M. 1958*a* *Mechanics*. Tokyo-tosho.

Landau, L. D. & Lifshitz, E. M. 1958*b* *Fluid Mechanics*. Tokyo-tosho.

Lundgren, T. S. & Mansour, N. N. 1988 Oscillations of drops in zero gravity with weak viscous effects. *J. Fluid Mech.* **194**, 479–510.

https://doi.org/10.1017/S0022112099005728 Published online by Cambridge University Press

Natarajan, R. & Brown, R. A. 1986 Quadratic resonance in the three-dimensional oscillations of inviscid drops with surface tension. *Phys. Fluids* **29**, 2788–2797.

Natarajan, R. & Brown, R. A. 1987 Third-order resonance effect and the nonlinear stability of drop oscillations. *J. Fluid Mech.* **183**, 95–121.

Rayleigh, Lord 1879 On the capillary phenomena of jets. *Proc. R. Soc. Lond.* A **29**, 71–97.

Reid, W. H. 1960 The oscillations of a viscous drop. *Q. Appl. Maths* **18**, 86–89. Tokyo Astronomical Observatory Edition 1985 *Chronological Scientific Table*. Maruzen Co., Ltd.

Trinh, E. & Wang, T. G. 1982 Large-amplitude free and driven drop-shape oscillations: experimental observations. *J. Fluid Mech.* **122**, 315–338.

Tsamopoulos, J. A. & Brown, R. A. 1983 Nonlinear oscillations of inviscid drops and bubbles. *J. Fluid Mech.* **127**, 519–537.

Yoshida, K., Amamiya, A., Ito, K., Kato, T., Matsushima, Y. & Furuya, S. (Eds.) 1967 *Ohyou Suugaku Binran (Handbook of Applied Mathematics)*. Maruzen.

Zhang, X. G. & Basaran, O. A. 1996 Dynamic of drop formation from a capillary in the presence of an electric field. *J. Fluid Mech.* **326**, 239–263.

https://doi.org/10.1017/S0022112099005728 Published online by Cambridge University Press